Available *online* at: http://ajeeet.ft.unand.ac.id/

Andalas Journal of Electrical and Electronic Engineering Technology

ISSN 2777-0079

Control, Automation, and Robotics

Estimation of the Shoulder Joint Angle Using Brainwaves

Minoru Sasaki [1,2], Takaaki Iida [1], Joseph Muguro [1,3], Waweru Njeri [1,2,3], Pringgo Widyo Laksono [1,4], Muhammad Syaiful Amri bin Suhaimi [1,5] and Muhammad Ilhamdi Rusydi [6]

[1] *Department of Mechanical Engineering, Gifu University, Yanagido 1-1, Gifu, 501-1193, Japan*
[2] *Intelligent Production Technology Research & Development Center for Aerospace (IPTeCA), Tokai National Higher Education and Research System,*
[3] *Department of Electrical & Electronic Engineering, Dedan Kimathi University of Technology, Private Bag, Nyeri 10143, Kenya.*
[4] *Department of Industrial Engineering, Universitas Sebelas Maret, Surakarta 57126, Indonesia*
[5] *National Institute of Technology, Gifu College, Gifu 501-0495, Japan*
[6] *Department of Electrical Engineering, Engineering Faculty of Universitas Andalas, Padang 25163, Indonesia*

ARTICLE INFORMATION

Received: April 21, 2021
Revised: May 1, 2021
Accepted: May 3, 2021

KEYWORDS

Shoulder Joint Angle; EEG; Neural Network

CORRESPONDENCE

Phone: +62 812-6156-6525
E-mail: sasaki@gifu-u.ac.jp

A B S T R A C T

This paper presents the angle of the shoulder joint as basic research for developing a machine interface using EEG. The raw EEG voltage signals and power density spectrum of the voltage value were used as the learning feature. Hebbian learning was used on a multilayer perceptron network for pattern classification for the estimation of joint angles 0°, 90° and 180° of the shoulder joint. Experimental results showed that it was possible to correctly classify up to 63.3% of motion using voltage values of the raw EEG signal with the neural network. Further, with selected electrodes and power density spectrum features, accuracy rose to 93.3% with more stable motion estimation.

INTRODUCTION

In the recent past, Japan and indeed the world, have witnessed a declining birthrate and aging of their population. This has caused an increase in the number of older adults in the country. In such a social situation, the burden on social welfare for the aged and the ill is heightened. It is highly desired to reduce the load on the caregiver by developing systems that support the independence of the care recipients. This system promotes the independence of the individuals and thereby improves the quality of life.

Devices that seek to increase, maintain and or improve the functional capability of the user are considered assistive technologies. In cases of disability or senility, the range of equipment's range from special communication devices, mobility devices like wheelchairs, hearing aids, control interfaces amongst others. Focusing on controlled devices, control schemes vary with different methodologies utilized in various research undertakings. Modalities like joystick control, input buttons, bio-signals, gesture recognition amongst others have been used.
In this research, the primary control mechanism has been on bio-signals owing to its ease of recording from different human body aspects. Among the biological signals, the approach using electroencephalography (EEG), electrooculography (EOG) and electromyography (EMG) methods are employed since they are less invasive with a considerable cost-effective measurement system.

EMG has been used by different authors in applications like ergonomics, prosthesis, robot controls, smart homes, muscle rehabilitation amongst others [1]–[4]. Similarly, EOG research targeting areas like robot control, human-machine interface, game control schemes, affective computing amongst others have been developed. EEG has found usage in locked-in patients who have lost motor control. Authors [5] and [6] used EEG to communicate with patients using speller tasks. Other brain-computer interfaces have been applied in varying fields [7]. Commercially, Research Laboratories have been developing a system that operate equipment using EEG signal, for example, moving electric beds and wheelchairs by measuring subtle changes in blood flow in the brain and sends the signal to electronic devices via a network [8], [9]. The Army Combat Capabilities Development Command's Army Research Laboratory has also shown interest in the usage of EEG towards cognition and ergonomics of military operations [10], [11]. Through this and other endeavors, a man-machine interface that uses a biomedical signal as an input is being actively developed.

https://doi.org/10.25077/ajeeet.v1i1.5

This research is focused on the EEG, which is said to be the highest order among biological signals to estimate the state of human shoulder movements. In other EEG studies, neural networks may be used for mental task classification and epileptic wave detection, but in this study, they are used for motion estimation. EEG contains a lot of information and is useful for the communication of elderly people and people with physical disabilities who place importance on intuition and low burden. Moreover, since the brain is the center of the nervous system, its function is likely to be maintained even in diverse age and illness-related complications. As such, there are many cases where EEG can be used even if the person becomes paralyzed or suffer from a stroke.

To record EEG, the setup involved the measurement of the surface potential of 14 lead-out sites on the scalp. The proposed system captures EEG signals emanating from arm motion to estimate shoulder movements using a neural network. As a preprocessing of the estimation, Fourier transformation is performed to make the characteristics of the EEG signal of each motion more conspicuous, considering changes in the physical condition of the subject and the measurement environment. The performance is experimentally evaluated using test subjects with a custom-built robot for visual feedback. Additionally, optimal electrode position is investigated to improve the accuracy of the proposal.

The rest of the document is organized as follows; Section 2 describes the methods applied where, EEG system setup, Fourier transformation and its usage in EEG feature extraction, as well as neural network training schemes, are described. In section 3, the results of the experiment are reported. In the section, motion estimation results and discussion are given for varying experimental settings. The paper ends with a conclusion that summarizes the findings and outlines the challenges and recommendations for further work.

METHODOLOGY

Electroencephalography (EEG) measurement

In literature, the brain is subdivided into four major lobes, Frontal, Parietal, Occipital, and Temporal lobes, which are tied to different bodily functions. The frontal lobe is generally mandated with higher executive functions including emotional regulation, planning, and problem-solving. Additionally, the region contains the primary motor cortex, the major region responsible for the voluntary movement of different body parts. The parietal lobe is largely responsible for integrating somatosensory information (touch, temperature, pain etc.). It also plays a part in coordinating hand-eye motions. The Temporal lobe on the other hand contains regions dedicated to processing the sensory information (hearing, recognizing language, etc.). Some regions of the temporal lobe also assist in making sense of complex visual information (in face recognition and scenes for example). Finally, the occipital lobe is considered the major visual processing centre of the brain. Located at the back portion of the brain, its role is interpreting visual stimuli and information. By recording brain activity, it is possible to discriminate which action the brain is executing. One such approach is the use of electroencephalography to record brain waves.

The electrical activity emanating from the spontaneous potential of the brain is referred to as EEG, a short form of Electroencephalogram. It is mainly recorded by electrodes placed on the scalp, sphenoid floor, eardrum, surface of the brain, deep brain, etc. Since EEG signals contain all physiological signals, albeit, at millivolt level at best, there is a possibility that complex motion can be identified with careful signal processing and analysis.

In this research, we used Kansei Spectrum Analysis System to investigate the waveform of EEG. EEG signal was recorded during arm motion, and the raw EEG is passed through Fourier transform for feature extraction. The extracted features were then fed to the multilayer perceptron (MLP) for classification. This is as shown in Fig. 1.

Fig. 2 shows the measurement equipment used and the electrode position configurations for data acquisition. Fig. 2(a) is the processor box for hardware digital filter processing, it processes EEG and provides a link to the PC for data import. Analog/Digital (A/D) conversion and amplification were performed on the raw signal by the EEG acquisition unit shown in Fig. 2(b). This device has 14 input channels and outputs the converted signal to the processing unit. For measurement, the electrodes were mounted at 14 locations as shown in Fig. 2(c) based on the international standard 10-20 method. All measurement methods were based on the right earlobe reference electrode lead. For repeatable positioning, the head cap is shown in Fig. 2(d) was used. The electrodes in use were dry leads, paste-less electrodes in the helmet. Table 1. below list the 14 EEG signals. The position for each electrode is represented as a combination of letters and numbers. The letter, in this case, represents the particular lobe i.e. Fp, Prefrontal lobe; F, Frontal lobe; T, Temporal lobe; C, Central lobe, P, Parietal lobe, and O, Occipital lobe. The numbers represent the skulls hemispherical location: Z, denotes the cerebral midline, even numbers represent the right hemisphere while odd numbers represent the left hemisphere.

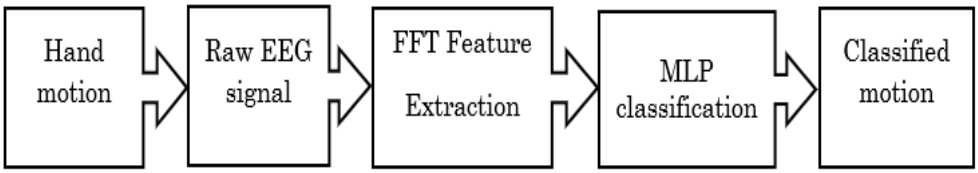

Figure. 1. Schematic Flow of the Proposal

 https://doi.org/10.25077/ajeeet.v1i1.5

Signal Processor Box

EEG Acquisition Box

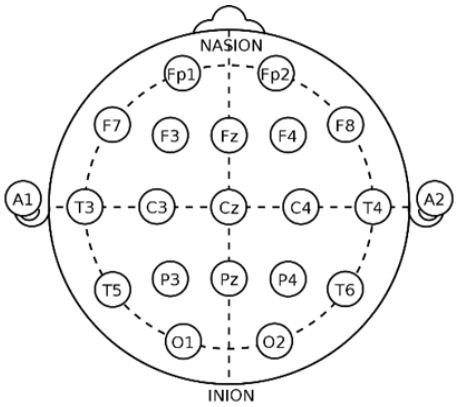

Electrode Placement

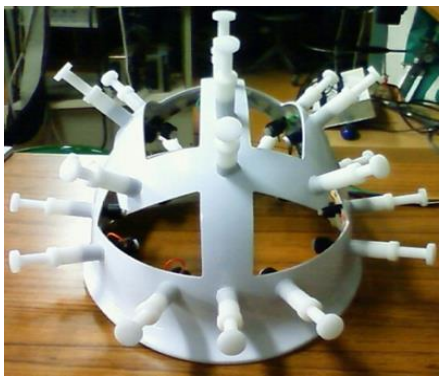

EEG Helmet

Figure 2. Data Acquisition Equipment and Electrode Connection

Table 1. Part Name and Anatomic Loci of Electrodes

Electrode symbol	Part name	Anatomical location
Fp1, Fp2	Pre-Frontal cortex/Frontal Polar	Frontal lobe
F3, F4	Frontal left/right	Frontal lobe (Motor area)
C3, C4	Central	Central groove
P3, P4	Parietal left/right	Parietal region (Somatosensory area)
O1, O2	Occipital	Occipital Lobe (Visual cortex)
F7, F8	Frontal	Lower forehead
T3, T4	Mid-Temporal	Middle temporal lobe
T5, T6	Posterior-Temporal	Temporal lobe
A1, A2	Earlobe (Auricular)	Ear
Fz	Midline Frontal	.
Cz	Midline center (Vertex)	
Pz	Midline Parietal	

Experimental setup

The experiment was conducted with test subjects seated comfortably in a chair with minimal movement to avoid motion artifacts. A baseline EEG was recorded with a rested arm, denoted in this article as the zero degrees (0º-0º), for 5 seconds. After a rest period of about 5 seconds to allow for saving the raw EEG file, the user proceeded with arm motion. The first motion involved performing a front raise, hold for a second before bringing it down. This is referred to as 0º-90° in this paper. The last motion was raising a hand to the highest possible position, holding and finally lowering. This is referred to as 0º-180° in the remaining part of the paper. In total, the experiment recorded EEG when the user performs three actions of the shoulder joint angle of the left arm; zero degrees (0°), zero degrees to ninety degrees (0°- 90°), and zero degrees to one hundred and eighty degrees (0° - 180°). The operation was repeated 10 times for each action, each lasting 5 seconds. Fig. 3 illustrates the experimental setup of the EEG based arm motion angle estimation.

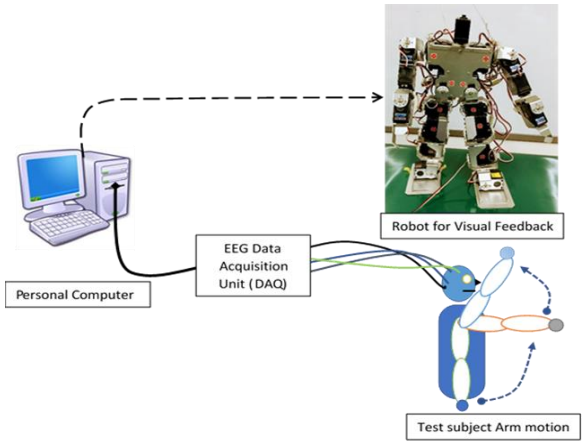

Figure 3. The Proposed System with Robot Control for Visual Feedback

MOTION ESTIMATION

The target of the research is motion estimation of the shoulder joint from the EEG signal. To this end, the raw EEG signal was passed through a preprocessing step for feature extraction. Several feature selection methods have been proposed in the literature; wavelet transforms, eigenvectors, time-frequency distributions, autoregressive models to name a few[12]–[14]. In this research, the two methods of feature extraction are investigated, one involving the raw EEG data and the other involving Fourier transformed EEG data. In Fourier transform feature extraction, the characteristics of the raw EEG signal to be analyzed is derived from power spectral density (PSD) estimation. This conversion was necessary to selectively represent the EEG sampled signal as well as reduce data dimensions [15], [16].

Power spectral density

When analyzing signal waveforms such as brain waves observed from the scalp due to the activity of many cells, it is often effective to evaluate the signal waveforms separately for each frequency component. This way, the signal was discretized at fixed time intervals (Δt). This is the so-called time discretization with sampling time, Δt. Which is also expressed as $1/\Delta t$, the sampling frequency.

After the discrete Fourier transform of the time series signal $x(n\Delta t)$ captured as a digital signal through the A/D converter to obtain $X(n\Delta f)$, the power spectrum $S(n\Delta f)$ is calculated from the expected value of the square of the amplitude for each frequency. When $1/T \equiv \Delta f$, the frequencies are discrete, i.e. Δf, $2\Delta f$, … The discrete Fourier transform of $x(m\Delta t)$ is given by eq (1).

$$X\left(n\Delta f\right)=\Delta t\sum_{m=0}^{T/\Delta t}x\left(m\Delta t\right)e^{2n\pi\Delta fm\Delta t} \tag{1}$$

$X(n\Delta f)$ is a complex quantity, but the absolute value of the complex number is the sum of the squared value of the real part and the squared value of the imaginary part and is expressed as eq (2).

$$\left|X\left(n\Delta f\right)\right|^2=\left(Re\left(X\left(n\Delta f\right)\right)\right)^2+\left(Im\left(X\left(n\Delta f\right)\right)\right)^2 \tag{2}$$

Therefore, the power spectral density $S(n\Delta f)$ is defined by eq (3) as shown.

$$S\left(n\Delta f\right)=\frac{1}{T}\left\langle\left|X\left(n\Delta f\right)\right|^2\right\rangle \tag{3}$$

Here $\langle|X(n\Delta f)|^2\rangle$ represents the average over several time series of length T. $S(n\Delta f)$ is the density of the power spectrum. The reason for the density is that when the sum is added from $f=n\Delta f$ to $m\Delta f$, it becomes the root mean square of the signals in that frequency range. The calculated power spectral density is fed to the neural network for training.

Multilayer perceptron

In analyzing EEG signals, artificial neural network models with different architectures have been employed in the literature. Support vector machines, radial basis function, adaptive neural-fuzzy, recurrent neural network, among others have been proposed with different amounts of processing time as well as accuracy [17]–[19]. In the paper, multilayer perceptron (MLP) architecture was applied as the neural network of choice.

A perceptron is a linear binary classifier used in supervised learning used to classify a given input data. It comprises of an input, weight, threshold, summer, and an activation function. A perceptron is a machine that outputs 1 when the input is a pattern P+ which exceeds the threshold and 0 when the input is a pattern P- which is less than the threshold. Alternatively, considering that there is only one output unit, the perceptron can be said to be a machine that divides the pattern appearing in the input layer into 1 and 0. Considering Fig. 4(a), the summed input to the unit u_j is expressed as

$$u_i=\sum_j w_jx_j-h_j \tag{4}$$

Where w_j correspond to the interconnection weight between j-th input and the neuron, x_i is the input pattern and h_j is the threshold. This way, feedforward pass is achieved. The output y_i is derived as shown in eq (5) by squashing the net input u_j using the Heaviside step function. The output value is converted into an output of 1 if the activation value is greater than or equal to the threshold, otherwise it is 0 as shown parametrically in equation 5.

$$y_i=H\left(u_i\right)=\begin{cases}1 & \text{if } u_i\geq 0\\ 0 & \text{otherwise}\end{cases} \tag{5}$$

The pictorial representation of the perceptron is as shown in Fig 4(a).

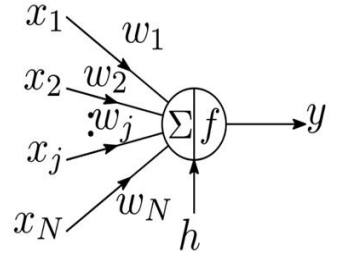

(a) Perceptron

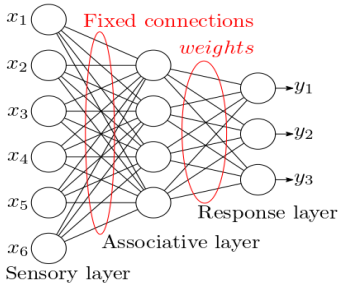

(b) Multilayer perceptron

Figure 4. Schematic View of the Perceptron

Multilayer perceptron derives its name from having a layered hierarchical network model comprising of a fully connected perceptron. Proposed by Rosenblatt in 1958, the perceptron is a model that uses the Hebbian learning rule using MacCullock-Pitts formal neurons and can acquire simple cognitive ability. In this

 https://doi.org/10.25077/ajeeet.v1i1.5

paper, a 3-layer NN was applied as shown in Fig. 4(b) having sensory layer(S), associative layer(A), and response layer(R). In other notation, the layers are described as the input layer, hidden layer, and output layer.

In this work, fixed connections were employed between the input nodes and the hidden units whereas interconnection weights were used between the hidden units and the output neurons.

Perceptron learning

Training multilayer perceptron is different from other multilayer architectures where techniques such as backpropagation are employed. Primarily, perceptron learning is expressed as a change in the weights from the hidden layer (association layer) to the output layer, whereas the weights from the input layer to the hidden layer are not considered.

The Hebbian learning algorithm is used where learning of the perceptron is expressed as a change in the coupling coefficient(weights) from the association layer to the reaction layer. During training, various input patterns are supplied as a teaching pattern in a supervised learning model. As these patterns are being propagated forward, the error arising from the difference between the output of any node *i* and the target value multiplied by the input to the neuron is proportional to the change required to make the pre-synapse and the post-synapse signals equal. Equation (6) shows the general learning rule (*delta rule*) of the MLP. In the expression, η is the learning rate, δ_i difference between the output of node i and the actual training value (i.e. error) while x_j is the input signal for the corresponding weight. It has enhanced the speed of convergence in that updating of the Hebbian synapse occurs at the same time as the occurrence of the difference between the presynaptic signal and the target value.

$$\Delta w_{ij} = \eta \delta_i x_j \tag{6}$$

Considering a training pattern c, with a corresponding input training signal t_c, the update formula of the weights for training can be expressed as in equation 7.

$$\begin{aligned} w_{ij}(n+1) &= w_{ij}(n) + \eta \Delta w_{ij}(n) \\ &= w_{ij}(n) + \eta\left(t_{c,j} - y_{c,j}\right) x_{c,j} \end{aligned} \tag{7}$$

In vector form, the expression can be converted to a recurrence formula as in (8).

$$\begin{aligned} w_{ij}(n+1) &= w_{ij}(n) + \eta \Delta w_{ij}(n) \\ &= w_{ij}(n) + \eta\left(t_{c,j} - y_{c,j}\right) x_{c,j} \\ w(n+1) &= w(n) + \eta\left(t_c - y_c\right) x_c \end{aligned} \tag{8}$$

Where $\boldsymbol{w(n)}$ is (w_1, w_2, ..., w_N) are the weight at the end of the n_th learning.

CLASSIFICATION OF PATTERNS USING MLP

Consider, an MLP network having two inputs and one output. The input to the networks is two sets of patterns P+ and P-. Such a network can be represented by a two-dimensional plane which is sometimes called the input space. Learning in a two-dimensional space involves finding the discriminant line that divides the space into subspaces occupied by the different patterns as shown in Fig. 5 below.

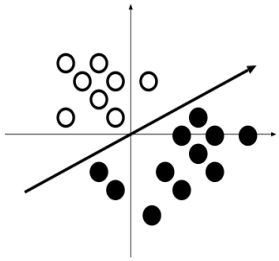

Figure 5. Input and the Distinction Straight Line of the Perceptron

Further, with the threshold assumed to be equal to zero, i.e. that the straight line that divides the two patterns into groups passes through the origin. The forward pass of the network will yield

$$\begin{aligned} 1 \text{ if} \quad & w_0 + w_1 x_1 + w_2 x_2 > 0 \\ 0 \text{ if} \quad & w_0 + w_1 x_1 + w_2 x_2 < 0 \end{aligned}$$

With $\mathbf{x} = [x_1, x_2]$ is the input vector and the vector $\mathbf{w} = [w_1, w_2]$ is the interconnection weight vector, the decision equations above are synonymous to determining whether the dot product of vector **w** and **x**, i.e. $\boldsymbol{w} \cdot \boldsymbol{x}$ is positive or negative. The dot product of the two vectors can also be expressed as

$$w \cdot x = w_1 x_1 + w_2 x_2 = |w||x| \cos\theta \tag{9}$$

Where the angle θ is the angle between the two vectors and can be expressed as.

$$\cos\theta = \frac{w \cdot x}{|w||x|} \tag{10}$$

The sign of the left-hand side of equation 7 depends on angle θ. The range in which θ is positive is between $-\pi/2 < \theta < \pi/2$ in radians. All the vectors in the shaded area in Fig 6 are normal to the weight vector and this line distinguishes between the groups, each having a different sense(sign) of the coupling elements of the elements. Within this range, for example, the dot product is positive, otherwise, the product will be negative.

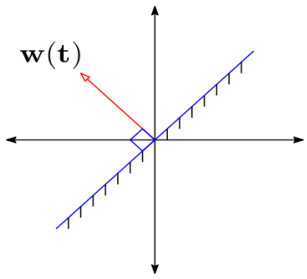

Figure 6. Learning Space and the Weight Vector

Graphically, consider three inputs $\mathbf{x}_1$, $\mathbf{x}_2$, and $\mathbf{x}_3$ in P+ and a randomly initialized weight vector w_0 as shown in Fig. 7(a). The boundary is the line perpendicular to the weight vector (shown in blue). From the figure, vector $\mathbf{x}_1$ is incorrectly classified. In the next learning iteration, the new weighting vector is $\mathbf{w}_1 = \mathbf{w}_0+\mathbf{x}_1$. This is accompanied by a new boundary that classifies $\mathbf{x}_3$ incorrectly as shown in Fig. 7(b). The next learning cycle aims to adjust the weight vector and thereby the boundary to have $\mathbf{w}_3$ in the correct subset. This is shown in Fig. 7(c) and is followed by vector $\mathbf{x}_1$ on the wrong side. In the final cycle shown in Fig. 7(d), $\mathbf{w}_3 = \mathbf{w}_2+\mathbf{x}_1$ changes the boundary such all the vectors are on the same side of the boundary which marks the end of the training.

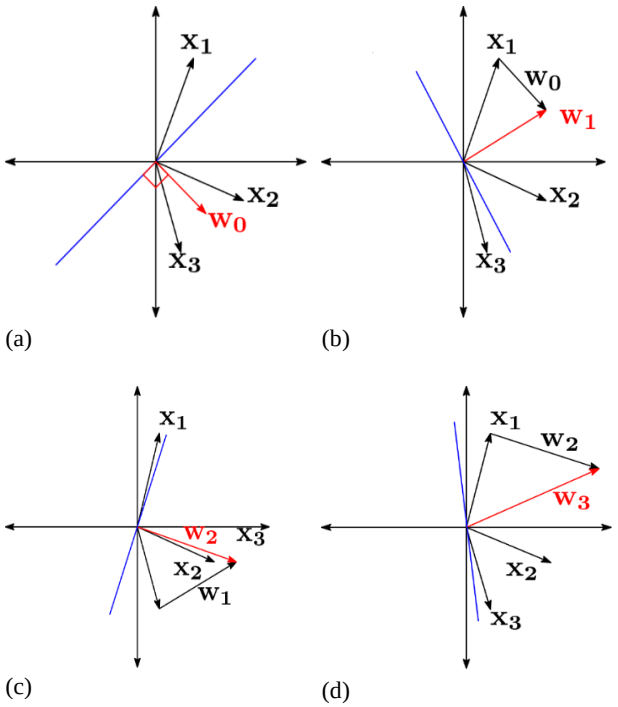

Figure 7. Graphical Representation of Perceptron Learning; (a) Initial Configuration, (b) Learning with x_1, (c) Learning with x_3, and (d) Learning with x_1

EXPERIMENTAL RESULTS AND DISCUSSION

Recorded raw EEG

Fig. 8(a) shows raw EEG data measured on a subject with the arm at rest or 0°- 0° movement for 14 channels labelled as Fp1, Fp2, F3, F4, C3, C4, P3, P4, O1, O2, F7, F8, T3, and T4 (see Fig 2c and Table 1) for 5 seconds. From the figure, there are weak signals in all the channels corresponding to other brain activities. The signals are uniform owing to the inactive state of the subject.

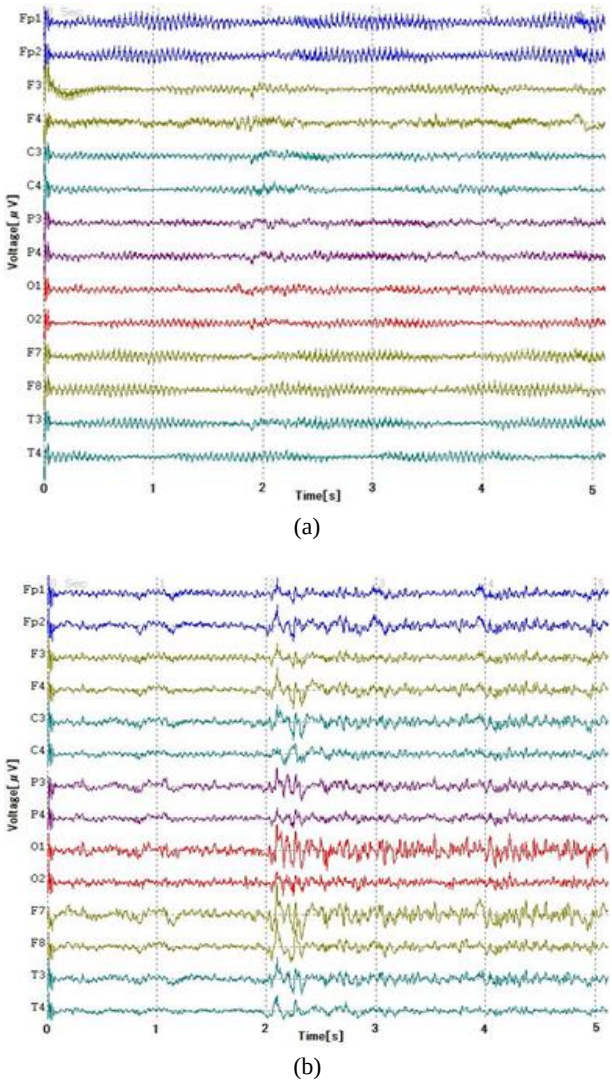

Figure 8. Results of EEG with the Left arm motion; (a) Zero degree (rested) arm motion, and (b) 0°- 90° arm motion

Fig. 8(b) shows EEG of arm motion for a 0°- 90° state. Unlike in Fig 5a which had a uniform signal throughout the experiment period, the signal amplitude increased and a change in the frequency distribution after 2 seconds into the experiment can be observed which are attributed to the brain activity resulting from the motion.

Fig. 9 shows the results of the 0°-180° arm movement. The resulting signals can be observed to be stronger than those generated by the 0°-90° arm motion. Similar to signals generated by the 0°-90°, these signals appear to have a random distribution relative to those obtained by the 0°-0°.

 https://doi.org/10.25077/ajeeet.v1i1.5

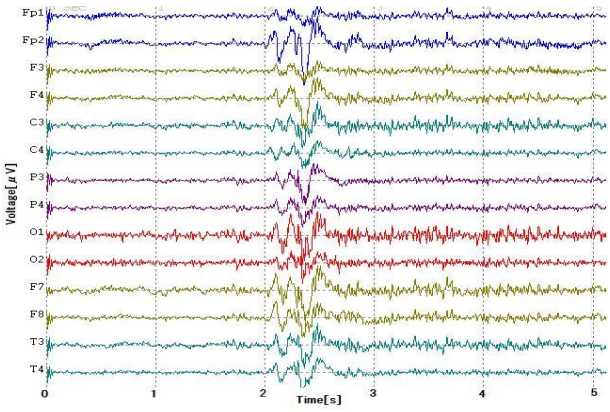

Figure 9. EEG of Left Arm Motion with 180-Degree (0°-180°-0°) Arm Motion.

From the results, the waveforms hardly changed for the 0°-0°. When arm motion was initiated, there is a significant increase in power for all the channels. Further, it was confirmed that the total potential for 0°-180° was larger than 0°-90°). From literature, the area in the brain occupied by shoulder movements is narrow, with motor effects appearing in a narrow range at the parietal region centering on the electrode positions of C3, C4, F3, F4, P3, and P4[20]–[22]. However, during the experiment, electrodes other than the frontal and parietal regions often showed significant changes as well. This is attributed to other brain functions associated with motion like motion coordination and visual feedback. As mentioned in section 2 above, the occipital region of the brain is critical in visual information processing. As the experiment is conducted, visual feedback as well as hand-eye coordination is required, soliciting EEG from at least all other brain regions.

The location of the action potential at 0°-90° and 0°-180° may change each time since EEG is stochastic in nature. The next subsection addresses this challenge by utilizing a machine learning model to predict motion.

Motion estimation

In motion estimation, the focus is on pattern recognition to discriminate active arm motion to overcome the problem of the stochastic nature of EEG in determining action potential locations. All 14 electrodes were used for learning and the performance was compared with and without feature extraction. At this time, a neural network was used as a pattern recognition method for discrimination. Additionally, optimal channels with clear discrimination were evaluated to reduce the number of channels needed.

Angle estimation with raw EEG signal

In this experiment, the raw EEG signal from the 14 electrodes was used for discrimination. For comparison and performance analysis, different neural network configurations were evaluated for optimal architecture. The number of input neurons was varied from 10 to 600 and the hidden neurons varied from 5 to 50 with each trial being repeated 10 times.

Fig. 10 below shows the response with 5 hidden neurons for a varying number of input neurons.

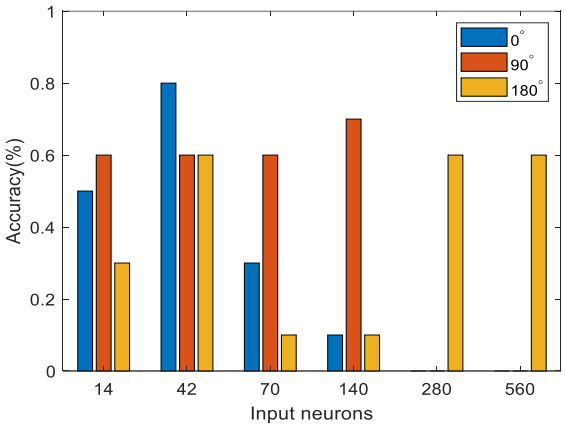

Figure 10. Performance with 5 Five Hidden Neurons

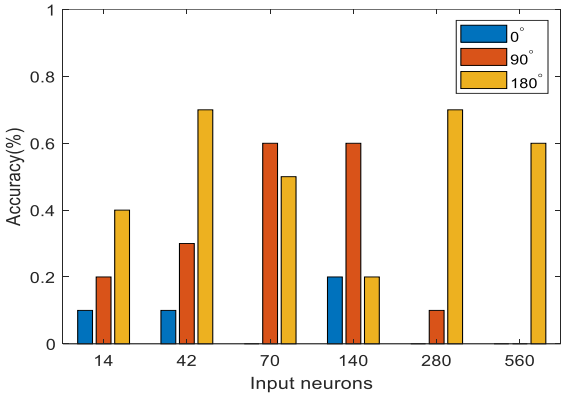

Figure 11. Performance with 10 Hidden Neurons

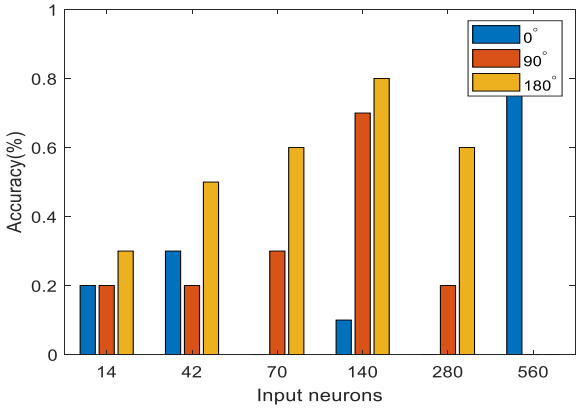

Figure 12. Performance with 50 Hidden Neurons

From Figures 10, 11, and 12, the use of 42 input neurons was found to have the best discrimination for the three motions. With 42 neurons in the input layer, the number of neurons in the hidden layer was varied to explore the optimal number of hidden neurons for the discrimination of the three motions.

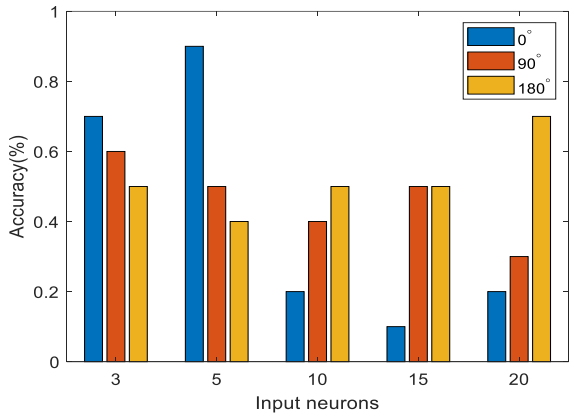

Figure 13. Performance of Discrimination with a Variable Number of Hidden Layers

Fig. 13 shows the performance of the network with 42 input neurons and a varying number of hidden neurons. From the results, it can be observed that the best performance, with better consistency, resulted with 3 hidden neurons with 70%, 60% and 50% for 0°-0°, 0°-90° and 0°-180° motion which average to 60% accuracy for the entire motion range.

Angle estimation with Fast Fourier Transform feature extraction

To obtain more prominent features for each motion, FFT of the raw EEG signal was performed before training. Fig. 14 below shows an example of the FFT of the Fp1 EEG signal for 0º-90º and 0º-180º motions. From the figure, it can be seen that the spectrum envelope of the two movements is the same, however, differences are present which will make it possible to discriminate between the two movements.

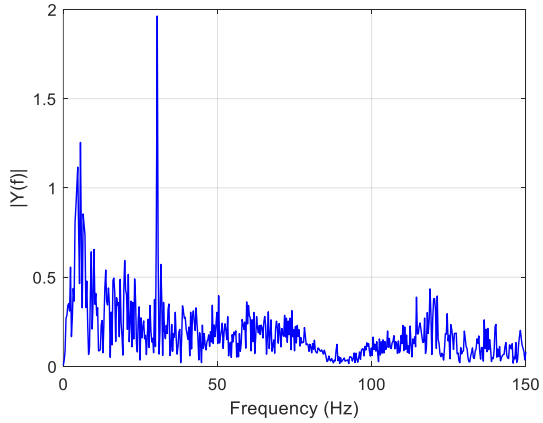

(a)

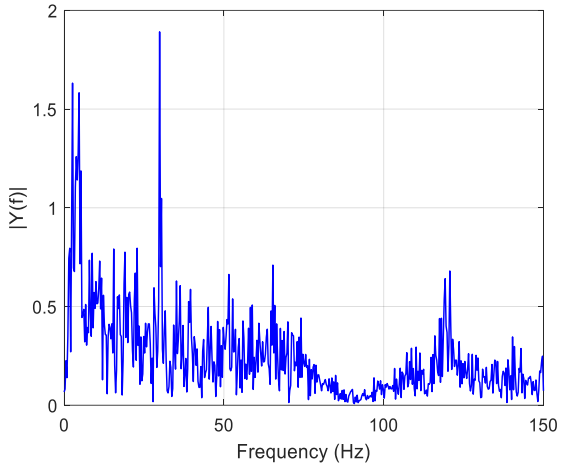

(b)

Figure 14. FFT Power Spectrum of Fp1 Signal; (a) 0º-90º Motion, and (b) 0º-180º Motion

Fig. 15 shows the quality of discrimination of the three joint angles with 1400 input neurons and a varying number of hidden neurons. The best performance in terms of accuracy was achieved with 5 hidden neurons.

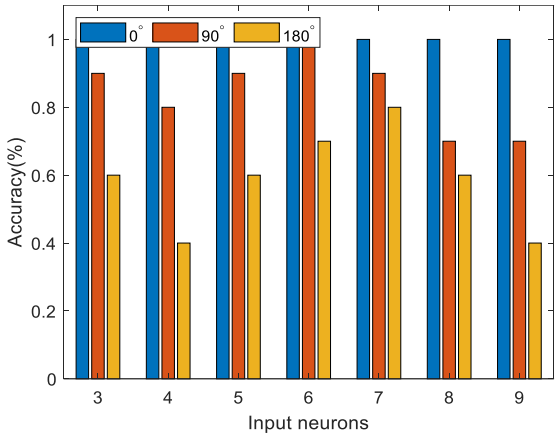

Figure 15. Performance of Classification Using FFT Feature Extraction

Selection of electrodes

Considering that different channels had different responses each time depending on the physical condition of the subject and other external factors, a preprocessing phase for motion estimation using a neural network was introduced. Preprocessing involved selecting a few channels with the largest instantaneous electrical potential for training the network.

Taking Fig. 16 as an example, the electrode that reacts most during the experiment is O1, followed by O2 and F7 in that order. Choosing these three signals for discrimination, training was carried considering signal strengths before and after the reaction as the characteristic quantities for discrimination.

 https://doi.org/10.25077/ajeeet.v1i1.5

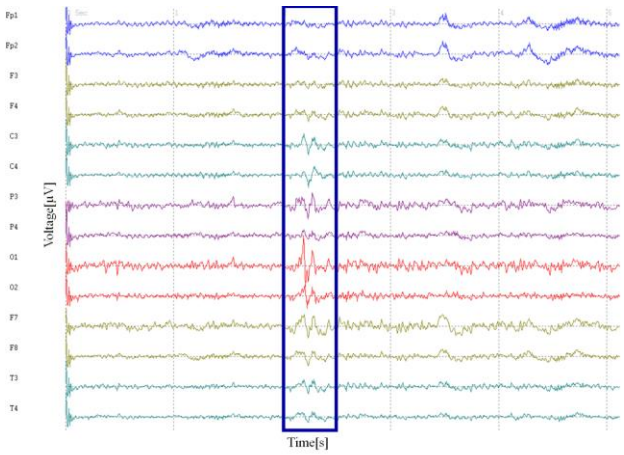

Figure 16. Selection of Electrodes

The performance of the angle classifier without and with channel selection and feature extraction using FFT power spectrum is as shown in Fig. 17 and Fig. 18, respectively.

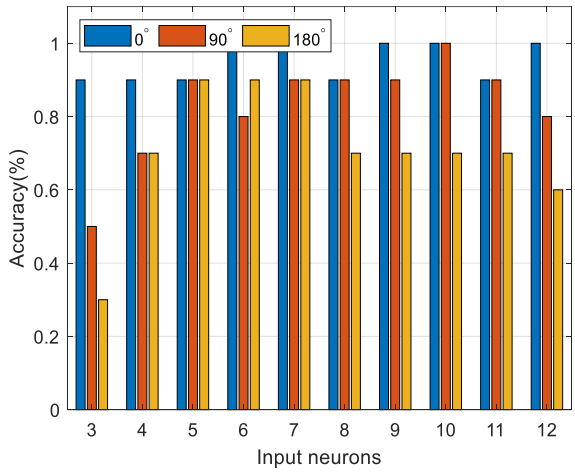

Figure 17. Angle Estimation from Raw EEG Data with Channel Selection

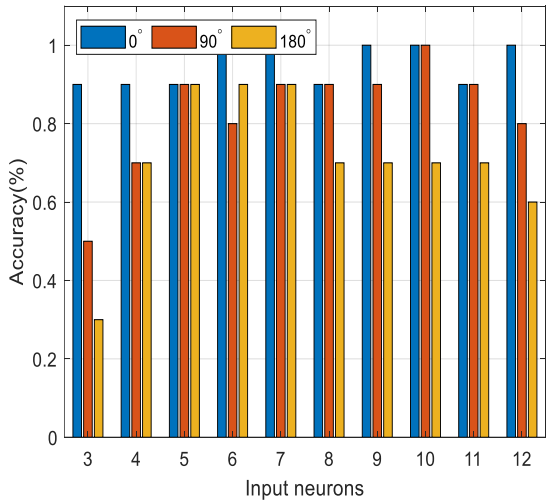

Figure 18. Angle estimation with channel selection and feature extraction using FFT

An improvement in motion classification for the three angles can be observed, with and without feature extraction when Figures 17 and 18 are compared with figures 13 and 15, respectively. From the results, 7 input neurons had the best performance of 90% for 0º-90º and 0º-180º and 100% for 0º-0º as shown in Fig. 17 & 18. This corresponds to an overall classification accuracy of 93% for the overall system. The improvement is attributed to the exclusion of signals with minimal or no variations as part of the training data.

CONCLUSIONS

This paper presented joint angle estimation by classifying EEG signals corresponding to three joint angles of the shoulder joint: 0º-0º, 0º-90º and 0º-180º. Multilayer perceptron neural network was trained using Hebbian learning to classify the electrode signals. Experiments involved the development of the algorithm and the determination of the optimal network architecture in terms of the neuron in the input and the hidden layer. Further, the performance of the classification system operating on raw EEG data was compared to the performance with feature extraction using FFT power spectrum with and without preprocessing. From the results, the optimal number of input neurons for a system trained with raw EEG signals was 42 neurons and 3 neurons in the hidden layer. Training with feature extraction yielded better results with the same number of hidden neurons albeit having 30-fold the number of input neurons. The performance of the classifier with channel selection outweighed the others that involved all the channels.

REFERENCES

[1] M. B. Kristoffersen, A. W. Franzke, C. K. van der Sluis, A. Murgia, and R. M. Bongers, "Serious gaming to generate separated and consistent EMG patterns in pattern-recognition prosthesis control," *Biomed. Signal Process. Control*, vol. 62, p. 102140, Sep. 2020, doi: 10.1016/j.bspc.2020.102140.

[2] N. Hooda, R. Das, and N. Kumar, "Fusion of EEG and EMG signals for classification of unilateral foot movements," *Biomed. Signal Process. Control*, vol. 60, p. 101990, Jul. 2020, doi: 10.1016/j.bspc.2020.101990.

[3] U. Orhan, M. Hekim, and M. Ozer, "EEG signals classification using the K-means clustering and a multilayer perceptron neural network model," *Expert Syst. Appl.*, vol. 38, no. 10, pp. 13475–13481, Sep. 2011, doi: 10.1016/j.eswa.2011.04.149.

[4] X. Chai *et al.*, "A hybrid BCI-controlled smart home system combining SSVEP and EMG for individuals with paralysis," *Biomed. Signal Process. Control*, vol. 56, p. 101687, Feb. 2020, doi: 10.1016/j.bspc.2019.101687.

[5] I. Lazarou, S. Nikolopoulos, P. C. Petrantonakis, I. Kompatsiaris, and M. Tsolaki, "EEG-based brain–computer interfaces for communication and rehabilitation of people with motor impairment: A novel approach of the 21st century," *Frontiers in Human Neuroscience*, vol. 12. Frontiers Media S. A, Jan. 2018, doi: 10.3389/fnhum.2018.00014.

[6] V. Guy, M. H. Soriani, M. Bruno, T. Papadopoulo, C. Desnuelle, and M. Clerc, "Brain computer interface with the P300 speller: Usability for disabled people with

amyotrophic lateral sclerosis," *Ann. Phys. Rehabil. Med.*, vol. 61, no. 1, pp. 5–11, Jan. 2018, doi: 10.1016/j.rehab.2017.09.004.

[7] H. G. Yeom, "Trends and future of brain-computer interfaces," in *Proceedings - 2018 Joint 10th International Conference on Soft Computing and Intelligent Systems and 19th International Symposium on Advanced Intelligent Systems, SCIS-ISIS 2018*, Jul. 2018, pp. 785–788, doi: 10.1109/SCIS-ISIS.2018.00130.

[8] J. Tang, Y. Liu, D. Hu, and Z. T. Zhou, "Towards BCI-actuated smart wheelchair system," *Biomed. Eng. Online*, vol. 17, no. 1, Aug. 2018, doi: 10.1186/s12938-018-0545-x.

[9] M. Aljalal, S. Ibrahim, R. Djemal, and W. Ko, "Comprehensive review on brain-controlled mobile robots and robotic arms based on electroencephalography signals," *Intelligent Service Robotics*. Springer, pp. 1–25, Jun. 2020, doi: 10.1007/s11370-020-00328-5.

[10] M. Chaouachi, I. Jraidi, and C. Frasson, "Modeling mental workload using EEG features for intelligent systems," in *Lecture Notes in Computer Science (including subseries Lecture Notes in Artificial Intelligence and Lecture Notes in Bioinformatics)*, 2011, vol. 6787 LNCS, pp. 50–61, doi: 10.1007/978-3-642-22362-4_5.

[11] C. Diaz-Piedra, M. V. Sebastián, and L. L. Di Stasi, "EEG Theta Power Activity Reflects Workload among Army Combat Drivers: An Experimental Study," *Brain Sci.*, vol. 10, no. 4, p. 199, Mar. 2020, doi: 10.3390/brainsci10040199.

[12] I. Nojima *et al.*, "Smaller muscle mass is associated with increase in EMG–EMG coherence of the leg muscle during unipedal stance in elderly adults," *Hum. Mov. Sci.*, vol. 71, p. 102614, Jun. 2020, doi: 10.1016/j.humov.2020.102614.

[13] M. M. Alam, A. A. Khan, and M. Farooq, "EFFECTS OF VIBRATION THERAPY ON NEUROMUSCULAR EFFICIENCY & FEATURES OF THE EMG SIGNAL BASED ON ENDURANCE TEST," *J. Bodyw. Mov. Ther.*, Jul. 2020, doi: 10.1016/j.jbmt.2020.06.037.

[14] M. Arunraj, A. Srinivasan, and S. P. Arjunan, "A Real-Time Capable Linear Time Classifier Scheme for Anticipated Hand Movements Recognition from Amputee Subjects Using Surface EMG Signals," *IRBM*, Aug. 2020, doi: 10.1016/j.irbm.2020.08.003.

[15] F. Artoni, A. Delorme, and S. Makeig, "Applying dimension reduction to EEG data by Principal Component Analysis reduces the quality of its subsequent Independent Component decomposition," *Neuroimage*, vol. 175, pp. 176–187, Jul. 2018, doi: 10.1016/j.neuroimage.2018.03.016.

[16] M. Taherisadr, M. Joneidi, and N. Rahnavard, "EEG Signal Dimensionality Reduction and Classification using Tensor Decomposition and Deep Convolutional Neural Networks," *IEEE Int. Work. Mach. Learn. Signal Process. MLSP*, vol. 2019-October, Aug. 2019.

[17] A. Subasi and E. Erçelebi, "Classification of EEG signals using neural network and logistic regression," *Comput. Methods Programs Biomed.*, vol. 78, no. 2, pp. 87–99, May 2005, doi: 10.1016/j.cmpb.2004.10.009.

[18] A. Craik, Y. He, and J. L. Contreras-Vidal, "Deep learning for electroencephalogram (EEG) classification tasks: A review," *Journal of Neural Engineering*, vol. 16, no. 3. Institute of Physics Publishing, p. 28, Apr. 2019, doi: 10.1088/1741-2552/ab0ab5.

[19] V. A. Maksimenko *et al.*, "Artificial neural network classification of motor-related EEG: An increase in classification accuracy by reducing signal complexity," *Complexity*, vol. 2018, 2018, doi: 10.1155/2018/9385947.

[20] S. Y. Kang *et al.*, "Brain networks responsible for sense of agency: An EEG study," *PLoS One*, vol. 10, no. 8, Aug. 2015, doi: 10.1371/journal.pone.0135261.

[21] C. Diniz *et al.*, "Mecanismos cognitivos e controle motor durante uma tarefa de movimento sacádico dos olhos: Evidências de eletroencefalografa quantitativa," *Arq. Neuropsiquiatr.*, vol. 70, no. 7, pp. 506–513, Jul. 2012, doi: 10.1590/S0004-282X2012000700007.

[22] F. Silva *et al.*, "Functional coupling of sensorimotor and associative areas during a catching ball task: A qEEG coherence study," *Int. Arch. Med.*, vol. 5, no. 1, p. 9, 2012, doi: 10.1186/1755-7682-5-9.

NOMENCLATURE

Δt	Sampling time
Δf	Sampling frequency
$X(n\Delta f)$	Power spectrum
$S(n\Delta f)$	Power spectral density
w_j	Interconnection weight
x_i	Input pattern
h_j	Threshold
u_j	Summed input
t_i	Target pattern
$H(u_i)$	Heaviside step function
Δw_{ij}	Difference between the presynaptic signal and the target value
η	Learning rate
δ_i	Error function of node i

AUTHOR(S) BIOGRAPHY

Minoru Sasaki

Minoru Sasaki is a Senior Professor at Gifu University, Faculty of Engineering, Intelligent Mechanical Engineering Course. He holds a Bachelor's degree from Yamagata University, Master and Doctorate degrees from Tohoku University, in Mechanical Engineering. He has collaborated with research institutions including KHI, University of California, Los Angeles, the Dedan Kimathi University of Technology among others. His current research interests include Intelligent Control, Mechatronics, and Robotics.

Iida Takaaki

Iida graduated with a Bachelor's and Master's degrees from Gifu University, Faculty of Engineering, Human Information Systems Engineering Department. He is currently working for Toyota Technical Development Company Co. Ltd. His current research interests include Intelligent Control and Mechatronics.

Joseph Muguro
Joseph Muguro is a PhD Fellow in the Faculty of Engineering, Gifu University, and a Lecturer at Dedan Kimathi University of Technology, Kenya. His research interest includes Machine Learning, Driver Behavior and Accident Analysis, among others.

Waweru Njeri
Waweru Njeri was a Post-Doctoral Fellow at Gifu University, and currently a Lecturer at the Dedan Kimathi University of Technology. Current research interests include Intelligent Control of Electro-Mechanical System, Robotics, and others.

Pringgo Widyo Laksono
Pringgo Widyo Laksono is a PhD Fellow in the Faculty of Engineering, Gifu University, and a Lecturer at the Department of Industrial Engineering, Universitas Sebelas Maret, Indonesia. His research interest includes Machine Learning, Bio-signals among others.

Muhammad Syaiful Amri bin Suhaimi
Amri bin Suhaimi graduated with a PhD from the Faculty of Engineering, Gifu University. He is now an Associate Professor at the National Institute of Technology, Gifu College, Gifu, Japan. His research interest includes Machine Learning, Robot control using Bio-signals among others.

Muhammad Ilhamdi Rusydi
Muhammad Ilhamdi Rusydi graduated with a PhD from the Faculty of Engineering, Gifu University. He is now an Associate Professor at the Department of Electrical Engineering, Engineering Faculty of Universitas Andalas, Padang, Indonesia. His research interest includes Machine Learning, Robot control using Bio-signals among others.